Influence of high-cycle fatigue on the tension stiffening behavior of flexural reinforced lightweight aggregate concrete beams

How-Ji Chen[1a], Te-Hung Liu[1b], Chao-Wei Tang*[2] and Wen-Po Tsai[1b]

[1]*Department of Civil Engineering, National Chung-Hsing University, Taichung 402, Taiwan*
[2]*Department of Civil Engineering & Engineering Informatics, Cheng-Shiu University, Kaohsiung 833, Taiwan*

Abstract. The objective of this study was to experimentally investigate the bond-related tension stiffening behavior of flexural reinforced concrete (RC) beams made with lightweight aggregate concrete (LWAC) under various high-cycle fatigue loading conditions. Based on strain measurements of tensile steel in the RC beams, fatigue-induced degradation of tension stiffening effects was evaluated and was, compared to reinforced normal weight concrete (NWC) beams with equal concrete compressive strengths (40 MPa). According to *applied load-mean steel strain* relationships, the mean steel strain that developed under loading cycles was divided into elastic and plastic strain components. The experimental results showed that, in the high-cycle fatigue regime, the tension stiffening behavior of LWAC beams was different from that of NWC beams; LWAC beams had a lesser reduction in tension stiffening due to a better bond between steel and concrete. This was reflected in the stability of the elastic mean steel strains and in the higher degree of local plasticity that developed at the primary flexural cracks.

Keywords: lightweight aggregate concrete; reinforced concrete beam; high-cycle fatigue; tension stiffening; bond-slip

1. Introduction

Reinforced concrete (RC) structures are often subjected to a high number of moderate stress level cycles (e.g., traffic, wave, and wind loads) during their service life. These types of repeated loads are within the high-cycle fatigue domain. A stabilized pattern of primary flexural cracks is generally expected to occur at service load levels, especially for RC flexural members (e.g., beams and slabs) (*fib* Bulletin 10 2000). The tensile concrete between these cracks contributes to reduce the steel strain. This bond-related phenomenon is often referred to as the tension stiffening effect (Stramandinoli and Rovere 2008, Dede and Ayvaz 2009). A decrease in the steel strain due to concrete can be considered as an increase in the stiffness of the

---

reinforcement compared to the bare bar. The rigidity of the cracked member varies from a minimum value at the cracked section to a maximum value midway between cracks. For simplification, the mean value along the axis of the cracked member is used in most code specifications (Eurocode 2 2004, CEB-FIP Model Code 1990 1993, ACI 318 2005). Consequently, knowledge of the mean steel strain is important in the analysis of load-deformation characteristics of RC members in the post-cracking range.

High-cycle fatigue is often a problem at service load levels for RC structures (ACI 215 1992). Even at conditions far from the ultimate limit state (ULS), long-term cyclic actions can affect the serviceability of RC members. This process is characterized by a significant increase in the total and permanent deformations (e.g., crack width and deflection) (Lovegrove and EI Din 1982). These deformations are mainly attributed to the progressive reduction of the bond between the concrete and the reinforcement (ACI 408 1992, Koch and Balázs 1992). The contribution of concrete between cracks (i.e., tension stiffening) is, therefore, reduced with the number of load cycles. The nonlinear and non-symmetrical behavior of the bond-slip mechanism results in a formation of irreversible relative slip. Although the reinforcement is within its elastic range at service load levels, residual strains along the reinforcement axis due to relative slip occur near cracks at the end of the unloading phase of each cycle (Fantilli and Vallini 2004, Zanuy *et al.* 2009, Ganesh Babu 1979). Moreover, the constituent materials of the RC member can be damaged under repeated loads by cyclic creep in compressive concrete and by cyclic strain softening of reinforcing steel (Balaguru and Shah 1982). The accumulation of internal defects (e.g., cracks and flaws) usually accompanies the degradation of mechanical properties (e.g., stiffness and strength). The reduction of tension stiffening and the evolution of fatigue damage are interrelated and have counteracting effects on the RC member. Isolating these phenomena from one another is difficult.

For many years, lightweight aggregate concrete (LWAC) with lower densities was used successfully for structural purposes because it reduced dead and seismic loads. In particular, for marine structures, LWAC must be used because of buoyancy considerations. Oscillatory stresses from wave action develop on these structures. Increasing interest in the use of LWAC in construction has generated many studies on the mechanical properties of LWAC (Mouli and Khelafi 2008, Ke *et al.* 2009). According to the results of pullout tests with different experimental configurations (Chen *et al.* 2004, Hossain 2008, Lachemi *et al.* 2009), the bond characteristics of LWAC are different from those in normal weight concrete (NWC). Due to the lower strength of the aggregate, the bond strength of LWAC is generally lower than that of NWC with the same compressive strength. Most design provisions require longer embedment lengths for LWAC to account for the lower bond strength.

Prior studies of LWAC bond characteristics only considered static loads. Several previous investigations (ACI 213 2003) concluded that the fatigue properties of plain LWAC were not significantly different from or comparable to those of NWC. In many instances, RC members with LWAC provided longer fatigue life. To the authors' knowledge, no studies concerning the cyclic bond behavior between steel and LWAC have been published. Specifically, the bond-related tension stiffening characteristics of LWAC in the high-cycle fatigue regime have not been investigated. In this study, we investigated the influence of high-cycle fatigue on the tension stiffening behavior of RC beams made with LWAC and with NWC by evaluating the strains of embedded tensile steels.
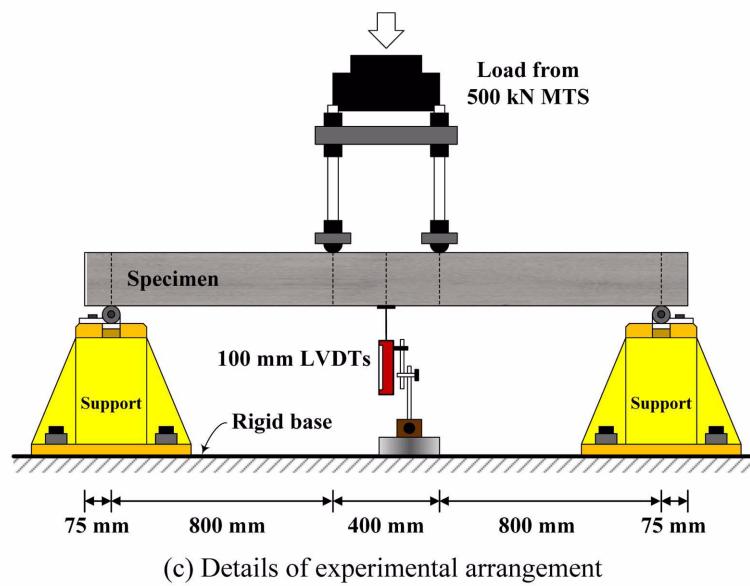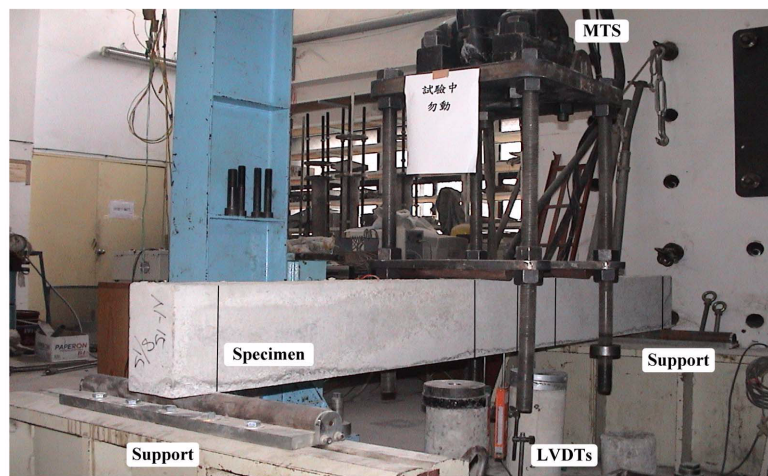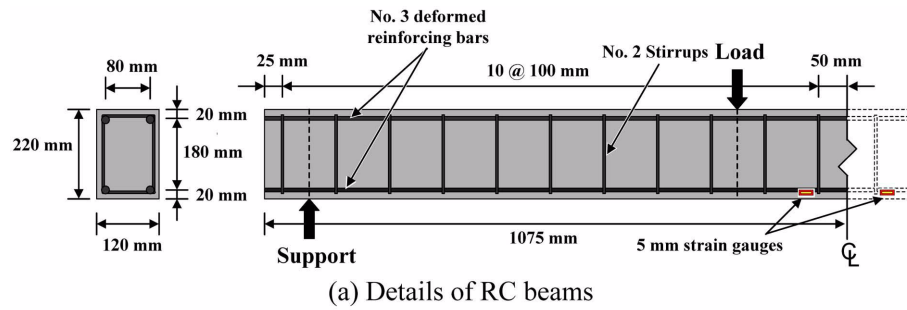
(a) Details of RC beams

(b) Photograph of experimental setup

(c) Details of experimental arrangement

Fig. 1 Loading and measurement apparatus for static load capacity and fatigue tests

Table 1 Properties of reinforcing steel

Bar	Nominal diameter (mm)	Yield stress (MPa)	Ultimate stress (MPa)	Elastic modulus (GPa)
No. 2	6.35	-	-	-
No. 3	9.50	398	545	200

Table 2 Mix proportions and fresh properties of concrete

Mixture	w/c	Cement (kg/m³)	Water (kg/m³)	Superplasticizer (kg/m³)	30-min absorption (kg/m³)	Aggregate (kg/m³)		Density (kg/m³)	Slump (mm)
						FA	CA		
LWAC	0.34	480	163	3.12	40	691	560	1934	80
NWC	0.52	377	196	0	-	667	1086	2325	85

Notes: CA = coarse aggregate; and FA = fine aggregate.

2. Experimental program

2.1 Test specimens and material properties

The details of the RC beams and their reinforcement layouts are shown in Fig. 1(a). The beams were 2.15 m long with 120 mm × 220 mm cross-sections. The arrangement of the reinforcing steel was the same for all RC beams. Number 3 deformed bars and number 2 plain rods were used for longitudinal and transverse reinforcement, respectively. The properties of the reinforcing steel, as provided by the manufacturer, are given in Table 1. Six LWAC and six NWC beams were fabricated. For each concrete mixture, two beams were used for static load capacity tests, and four beams were used for fatigue tests of various cyclic load levels.

Both the LWAC and NWC mixtures were designed to achieve a 28-day compressive strength of 40 MPa, and strengths were verified through trial batches. The resulting mix proportions of concrete are given in Table 2. Locally manufactured ASTM Type I Portland cement with a specific gravity of 3.15 and a fineness of 3400 cm²/g was used. A "G-type" high-range water reducer (superplasticizer) with a specific gravity of 1.2 was used in the LWAC mixes to improve workability. In the NWC mixes, natural river gravel and sand were used as coarse and fine aggregates, respectively. The maximum coarse aggregate size was 19 mm. Lightweight expanded shale aggregate was used as coarse aggregate for the LWAC with the same natural sand. The physical properties of the natural and lightweight aggregates are summarized in Table 3. The mechanical properties of plain concrete, tested in accordance with ASTM specifications, are shown in Table 4. Cylinders (100 mm in diameter and 200 mm in height) were used for compression tests (compressive strength and elastic modulus), and prisms (100 mm wide × 100 mm deep × 360 mm long) were used for flexural tests (modulus of rupture). Due to the weaker aggregates, the LWAC had an elastic modulus and a modulus of rupture that were 26% and 17% lower, respectively, than those of the NWC with equal compressive strength (Table 4).

All specimens, including the RC beams and plain concrete specimens, were cast and left in a steel mold for one day, and were then demolded and stored in a standard curing room with an average ambient temperature of 23±1.1ºC and a relative humidity of 100% for 28 days. After the curing

Table 3 Physical properties of aggregates

(a) Natural aggregate

Type	Density (SSD) (kg/m^3)	Absorption (SSD) (%)	Dry-rodded density (kg/m^3)	FM
CA	2590	1.57	1577	-
FA	2680	0.98	-	2.71

Notes: CA = coarse aggregate; FA = fine aggregate; SSD = saturated surface dry condition; and FM = fineness modulus.

(b) Lightweight aggregate

Grain size (mm)	Density (OD) (kg/m^3)	Absorption (%)		Particle crushing strength (MPa)
		30 mins	24 hrs	
5-19	1410	7.1	10.5	8.6

Notes: OD = oven dry condition.

Table 4 Mechanical properties of hardened concrete

Mixture	Compressive strength (MPa)				Elastic modulus (GPa)		Modulus of rupture (MPa)	
	7-day		28-day		28-day		28-day	
LWAC	38.4 37.6 37.1	(37.7)	39.8 41.9 40.9	(40.8)	22.4 23.1 22.7	(22.7)	6.0 5.4 5.7	(5.7)
NWC	31.6 33.4 32.6	(32.5)	40.6 40.6 40.8	(40.7)	30.5 29.8 31.1	(30.5)	6.9 7.1 6.7	(6.9)

process, the plain concrete specimens were air dried for one day, and the RC beams were air dried for at least one month prior to testing.

2.2 Loading and measurement apparatus

The experimental setup is shown in Fig. 1(b). A hydraulic servo-controlled testing machine, with a load capacity of 500 kN and a stroke range of 250 mm, were used in both the static load capacity tests and the fatigue tests with the same loading arrangement (Fig. 1(c)). Specimens were tested using a four-point loading method with a shear-span-to-depth ratio (a/d) of 4. This ensured flexural failure. During loading, the elongation of the tensile reinforcing steel within the pure bending region (between the two loading points) was measured by two 5-mm strain gauges attached to the steel surface (Fig. 1(a)). The mean steel strain was calculated by averaging the measured values of the two strain gauges. The beam deflection at midspan was measured by two 100-mm linear variable differential transducers (LVDTs). The outputs of the LVDTs, the strain gauges, and the load cell (actuator force) and the stroke of the testing machine were collected with a high-speed data acquisition system.
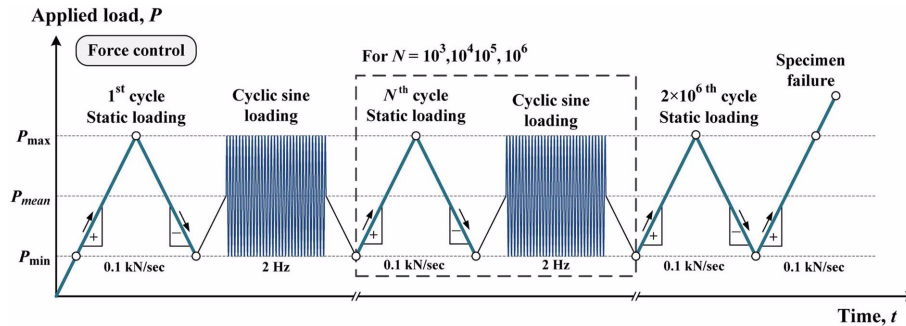
Fig. 2 Loading history for fatigue tests

2.3 Test procedures

2.3.1 Static load capacity tests

The static load capacity determined the maximum cyclic load (i.e., the allowable range of cyclic load) used in fatigue testing. Static load capacity tests were performed up to specimen failure using force control, a constant monotonic loading rate of 0.1 kN/sec, and a data acquisition rate of 1 Hz. For safety considerations, an interlock mechanism was set by the control system. Once the maximum actuator movement of 70 mm was reached, the testing machine stopped automatically.

2.3.2 Fatigue tests

The experimental configurations for fatigue testing were identical to the static load capacity tests. The loading history (force control) for the fatigue tests is shown in Fig. 2. Two types of loading, static and cyclic, were adopted in the fatigue tests. Cyclic loading in the form of unidirectional sinusoids started at the level of mean cyclic load (P_{mean}) and temporarily paused after a specific number of cycles. A constant cyclic load range (P_r) and a constant load frequency of 2 Hz were applied. Prior to fatigue testing, the load frequency was determined from the performance curve of the testing machine. The potential range of the actuator force and movement for a given load frequency exceeded experimental demands. During cyclic loading, data were continuously recorded at an acquisition rate of 0.017 Hz. Static loading was applied at $N = 1$, 10^3, 10^4, 10^5, 10^6, and 2×10^6 cycles with the same loading and data acquisition rates (i.e., 0.1 kN/sec and 1 Hz, respectively) as the static load capacity tests. After 2 million cycles, the specimens were statically loaded to failure.

Analysis of the residual load capacity of the tested RC beams after fatigue testing was beyond the scope of this study. Fatigue testing of each specimen took approximately twelve days. For routine maintenance, the testing machine was allowed to rest for at least one day before fatigue testing of the next specimen was initiated. Generally, for RC members under service conditions, a fatigue life of 2 million cycles is admissible for most structural applications (Oh *et al.* 2003).

3. Theoretical model and analytical methods

3.1 Eurocode 2 (EC 2) model for cracked RC members

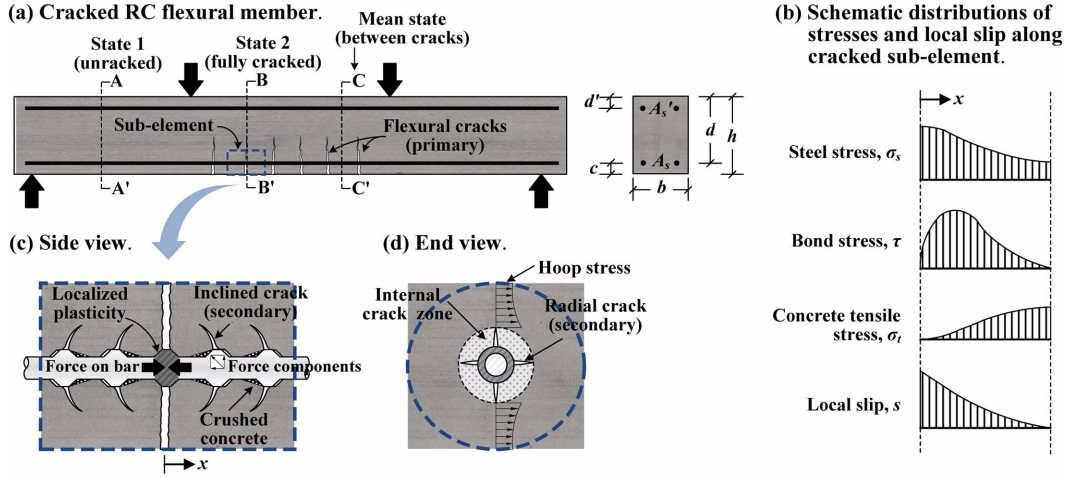Current code provisions, such as Eurocode 2, CEB-FIP model code 1990 and ACI 318, use

Fig. 3 Cracking mechanism and bond-related tension stiffening in RC flexural members

similar, slightly modified approaches based on the *total* monotonic response and the simplified coefficients to evaluate mean steel strains (ε_{sm}) in cracked RC members. Estimating residual values under repeated loading using these codes is not possible because the unloaded state cannot be reproduced by the codes. The cracking mechanism of an RC member subjected to a bending moment or an axial force, according to the Eurocode 2 (EC 2) method, is shown in Fig. 3. The mean steel strain (ε_{sm}), which lies between the strain of an uncracked section (State 1) and that of a fully cracked section (State 2), can be expressed as

$$\varepsilon_{sm} = (1 - \zeta)\varepsilon_{s1} + \zeta\varepsilon_{s2} \tag{1}$$

where, ε_{s1} and ε_{s2} are the steel strains in States 1 and 2, respectively; and ζ is a dimensionless coefficient representing the extent of cracking. $\zeta = 0$ for an uncracked section, and $0 < \zeta < 1$ for a cracked section. The value of ζ is given by

$$\zeta = 1 - \beta_1\beta_2\left(\frac{\sigma_{s,cr}}{\sigma_s}\right)^2 = 1 - \beta_1\beta_2\left(\frac{P_{cr}}{P}\right)^2 \tag{2}$$

where, $\sigma_{s,cr}$ and σ_s are the stresses in the tensile steel calculated on the basis of a fully cracked section under the cracking load P_{cr} and the load P, respectively; and β_1 and β_2 account for bond characteristics ($\beta_1 = 1$ for ribbed bars, and $\beta_1 = 0.5$ for plain bars) and the nature of the loads ($\beta_2 = 1$ for short-term loads, and $\beta_2 = 0.5$ for long-term or repeated loads).

To obtain the mean steel strain (ε_{sm}) in an RC flexural member, the transformed-section method, which is a convenient procedure for analyzing the bending stresses in a composite RC beam, can be used. The steel strain (ε_{si}) in State i can be computed with Eq. (3) based on the loading arrangement used.

$$\varepsilon_{si} = n\frac{P/2 \cdot a \cdot (d - y_i)}{E_s I_i}; \quad i = 1 \text{ for State 1, and } i = 2 \text{ for State 2} \tag{3}$$

where a is the shear span length; E_s is the elastic modulus of reinforcement; n is the modular ratio

of reinforcement to concrete; y_i is the distance from the extreme compressive fiber to the neutral axis in State i; I_i is the moment of inertia of the transformed section in State i; and d is the effective depth from the extreme compressive fiber to the centroid of the tensile steel.

3.2 Typical behavior of RC beams under monotonic and cyclic loads

A comparison of the typical behavior of RC beams under monotonic and cyclic loads is shown in Fig. 4. Due to the relatively lower cracking load (P_{cr}), the primary flexural cracks usually occurred during the first cycle before the maximum cyclic load (P_{max}) was reached. The cracking state of the RC beams was steady until fatigue failure (Fig. 3(a)). The non-uniform distributions of steel stress and local slip along the cracked RC member in the region adjacent to the crack caused by initial cracking are illustrated in Fig. 3(b). Because local slip between steel and concrete is irreversible, the residual tensile stresses and strains remained in the reinforcement after unloading. The total mean steel strain response in the RC beams can be divided into elastic and residual parts as follows

$$\varepsilon_{smT,N} = \varepsilon_{smE,N} + \varepsilon_{smR,N} \tag{4}$$

where, $\varepsilon_{smT,N}$, $\varepsilon_{smE,N}$ and $\varepsilon_{smR,N}$ are the total, elastic and residual mean steel strains, respectively, at N cycles.
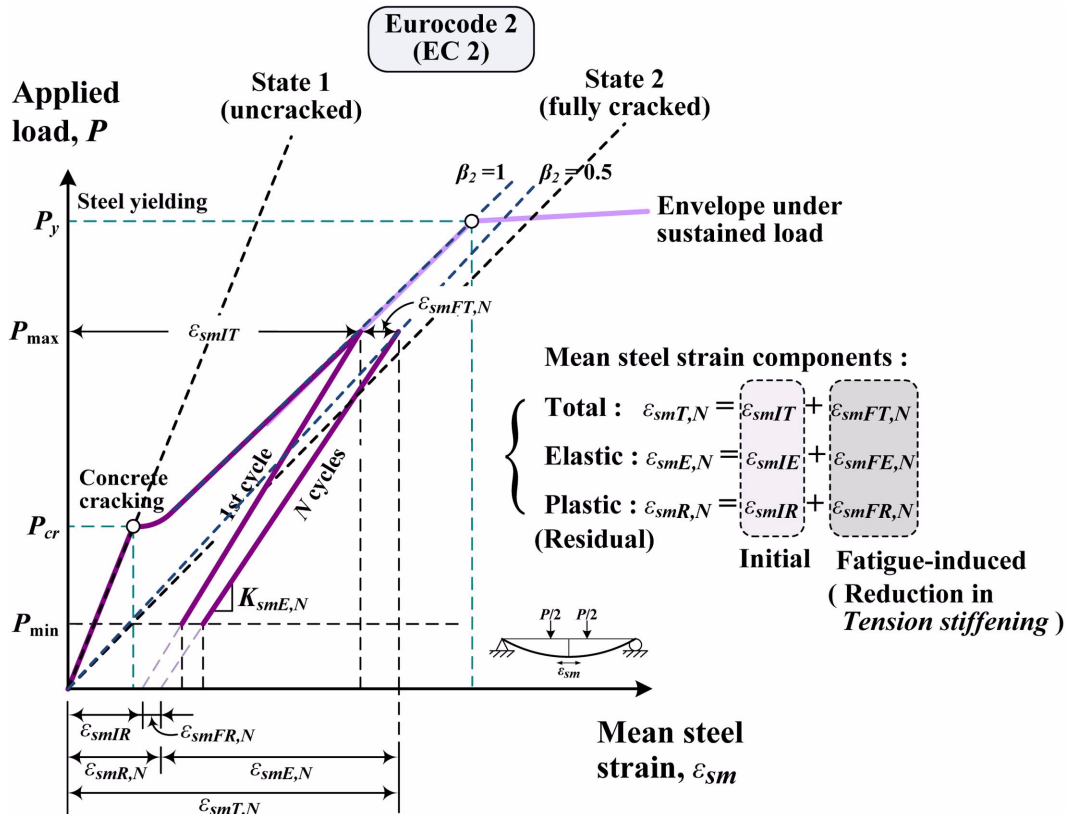

Fig. 4 Typical *applied load-mean steel strain* diagram of RC flexural members under monotonic and non-reversed cyclic loading

(a) Crack direction normal to bar axis   (b) Crack direction parallel to bar axis (bare bar)
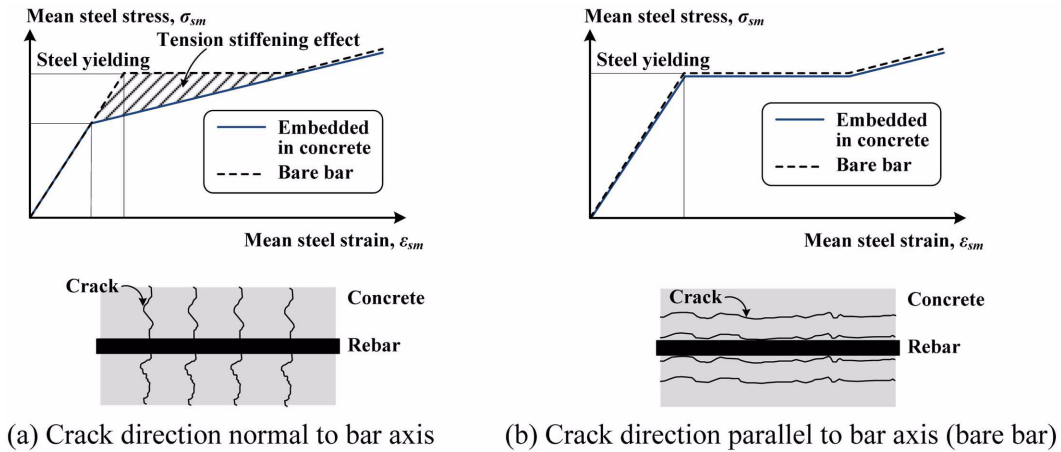
Fig. 5 Typical yield strength of tensile steel embedded in concrete

With load cycles, decreases in tension stiffening due to the development of secondary bond cracks (Figs. 3(c) and (d)) in the concrete between primarily flexural cracks led to an increase in the mean steel strain and other related member properties (e.g., flexibility, deflection and crack width). Therefore, the true effects of high-cycle fatigue on the RC beams (i.e., deviations from the envelope under sustained static loads) should be considered to start from the unloading stage of the first load cycle after initial cracking. In this study, fatigue-induced changes in the mean steel strain as a function of the number of cycles were distinguished from initial changes (independent of the number of cycles) according to the following expression

$$\varepsilon_{sm\lambda, N} = \varepsilon_{smI, \lambda} + \varepsilon_{smF\lambda, N} \tag{5}$$

where, $\varepsilon_{smI, \lambda}$ and $\varepsilon_{smF\lambda, N}$ are the initial part (at first cycle) and the fatigue-induced part (at N cycles) of the mean steel strain, respectively; and the subscript λ represents the total ($\lambda \to T$), elastic ($\lambda \to E$) and residual ($\lambda \to R$) mean steel strains.

Tension stiffening effects are often reflected in the reduced average yield strength and strain of the tensile steel embedded in the concrete compared to the bare bar (Fig. 5) (Maekawa *et al.* 2003). Relatively higher stresses and strains can be found at the primary flexural cracks. Particularly for the case of cyclic load conditions, localized plasticity of reinforcement might have occurred in the vicinity of the primarily flexural cracks (Fig. 3(c)) prior to the achievement of an average yield state.

On the other hand, tension stiffening effects are also associated with the crack softening characteristics of concrete. This behavior can be studied by the *local stresscrack width* response of concrete at the crack determined in the deformation-controlled tensile tests. Based on the fracture mechanics of concrete, the mathematical models (e.g., the fictitious crack model) for crack tip modeling can be established. Cornelissen *et al.* (1986) performed four types of uni-axial tests with lower levels of 0%, -10%, -15% and 100% of tensile strength on NWC and LWAC. Differences in behavior, including the envelope curves and the post-peak cyclic behavior, of the two types of concrete were compared. The strength of LWAC was limited by its weaker aggregates, and the cracks passed through the aggregate particles (i.e., the smoother crack surface). Conversely, cracks in NWC propagated along grain surfaces and allowed sliding friction. For this reason, load transfer
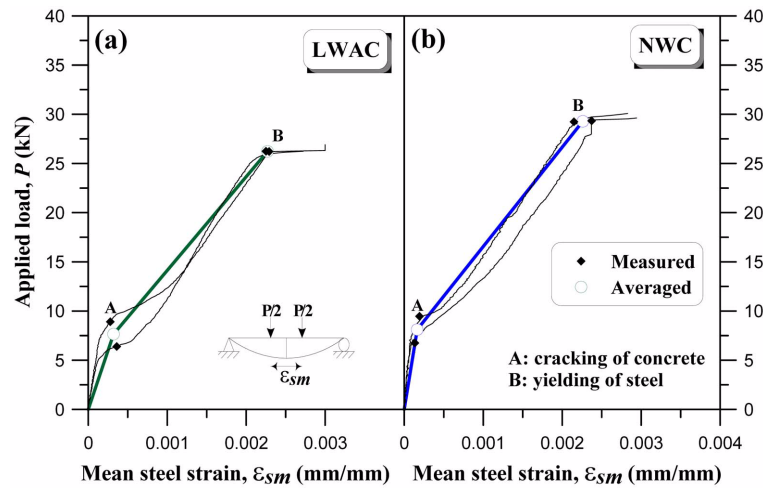
Fig. 6 *Applied load-mean steel strain* curves of RC beams under static loading

and fracture energy for LWAC were less than those for NWC, whereas the tensile envelope curves were not significantly affected by cyclic loading.

However, the softening capacity of concrete at cracks can be neglected due to its rapid deterioration in the high-cycle fatigue domain (Zanuy *et al.* 2010). This is consistent with the assumption made in most design codes that the load is fully carried by the reinforcement at the crack (State 2).

4. Results and discussion

4.1 Static load capacity tests and determination of yield load

Two beams from each concrete mixture (i.e., LWAC and NWC) were loaded to failure. The load was plotted against the mean steel strain to 4,000 μ (Fig. 6). The relevant state points (i.e., cracking and yielding) of the RC beams could be verified from the *applied load-mean steel strain* curves. The representative values of the LWAC and NWC beams were obtained from the average load of the two specimens.

Under the same static load, the lower elastic modulus of LWAC (Table 4) resulted in a higher mean steel strain in the LWAC beams (Fig. 6). Additionally, a lower average cracking load (P_{cr}) was observed in the LWAC beams. The cracking load of the tested RC beams depended mainly on the modulus of rupture of plain concrete (Table 4).

Further, the average yield load (P_y) of LWAC beams (26.23 kN) was lower than that of the NWC beams (29.28 kN). The calculated average yield strengths of the tensile steel embedded in LWAC and NWC were 359 MPa and 394 MPa, respectively (Figs. 7(a) and (b)). These calculations were based on the Eurocode 2 (EC 2) method, with reinforcement properties given in Table 1. The earlier yielding of tensile steel in the LWAC beams could be attributed to the larger difference in the elastic modulus between LWAC and steel (i.e., a higher distributed steel stress) and the contribution of
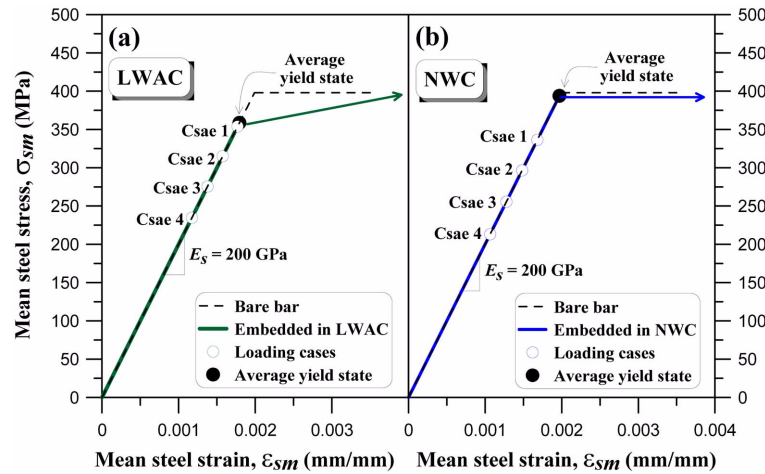
Fig. 7 Calculated average stress-strain relationships of tensile steel in RC beams
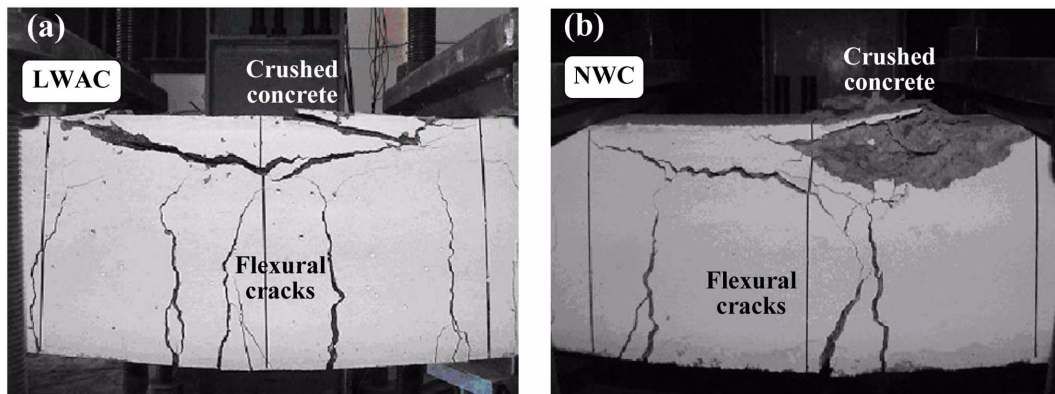

Fig. 8 Crack patterns of RC beams after static load capacity tests

tension stiffening effects (Fig. 5). Mor (1992) and Mor *et al.* (1992) indicated that the improved elastic compatibility of the lightweight aggregate particles to the surrounding mortar matrix (i.e., similar elastic modulus of the constituent phases) could effectively reduce internal damage to the LWAC (i.e., micro-cracking and secondary bond cracks, as illustrated in Figs. 3(c) and (d)). Therefore, improved tension stiffening was provided by the improved bond between steel and concrete in LWAC.

After steel yielding, the *applied load-mean steel strain* curves of the RC beams tended to become flat. The tested RC beams experienced flexural failure (i.e., pull-out of tension steel followed by the crushing of concrete in the compression zone). The crack patterns of the RC beams after static load capacity tests are shown in Fig. 8. There was no significant difference in the visible crack patterns between the LWAC and NWC beams.

The maximum applied cyclic load (P_{max}) adopted in the fatigue tests should be lower than the average yield load (P_y) of the RC beams. The fatigue loading values are listed in Table 5. Four

Table 5 Determined values of applied cyclic loads

Cyclic load level	P_{mean} (kN)	P_{max} (kN)	P_{min} (kN)	P_r (kN)	Frequency of load (Hz)
Case 1	17.95	25.95	9.96		
Case 2	15.71	23.70	7.71		
Case 3	13.46	21.46	5.47	16	2
Case 4	11.22	19.21	3.22		

Notes: P_{mean} = mean cyclic load; P_{max} = maximum cyclic load; P_{min} = minimum cyclic load; and P_r = range of cyclic load.

levels (Cases 1 to 4) of mean cyclic load (P_{mean}) with a constant cyclic load range of 16 kN were used in the fatigue tests. The design goal of the fatigue tests was to assess the degradation characteristics of the RC beams at various cyclic load levels in the high-cycle fatigue domain with respect to the evolution of increases in steel strain.

4.2 Fatigue tests

4.2.1 Fatigue behavior of RC beams during cyclic loading

None of the beams failed prior to 2 million cycles. However, after at least 10,000 cycles in most cases, the strain gauges failed during the period of cyclic loading, although the strain gauge capacity for monotonic loading (approximately 3,000 μ, Fig. 6) was not exceeded. This could be caused by the interaction between the steel and concrete. The strain gauges attached to the tensile steel surfaces may have been gradually damaged by the surrounding concrete. Due to this experimental difficulty, a limited amount of data from the gauge measurements was available. Nevertheless, meaningful characteristics for the behavior of tensile steel during fatigue were provided.

Fatigue test results are shown in Fig. 9 for LWAC beams and in Fig. 10 for NWC beams. Based on the method described in Section 3.2, the development of mean steel strain with load cycles was plotted according to the *applied load-mean steel strain* curves for the RC beams. The contribution of the strain components (i.e., the elastic and residual parts) and the oscillating strains at the minimum, mean and maximum cyclic loads to the total mean steel strain were clearly visible. In Figs. 9 and 10, a similar trend between the growths of the statically and dynamically measured mean steel strains is shown. The range of dynamically measured mean steel strains was generally lower than that of the statically measured strains. Because of the effects of different loading rates, smaller steel strains were recorded in the RC beams under dynamic conditions with higher loading rates.

After initial cracking of the RC beams, the concrete between adjacent primary cracks was still capable of carrying considerable tensile force and offering stiffness due to the bond between the steel and concrete (i.e., tension stiffening). The *applied load-mean steel strain* curves (Figs. 9 and 10) at the unloading stage of the first load cycle were relatively nonlinear and gradually became linear for subsequent load cycles. This implied that the tensile force was increasingly dominated by the reinforcing steel after an increased number of cycles. This may explain why most of the fatigue failure of flexural members of RC and partially prestressed concrete (PC) is dominated by reinforcement fracture, although the concrete in compression in these members may be critical at static and low-cycle repeated loads (i.e., low-cycle fatigue) (Lenschow 1982). In addition,

(a) Loading Case 1 (P_{mean}=17.95 kN)

(b) Loading Case 2 (P_{mean}=15.71 kN)

(c) Loading Case 3 (P_{mean}=13.46 kN)
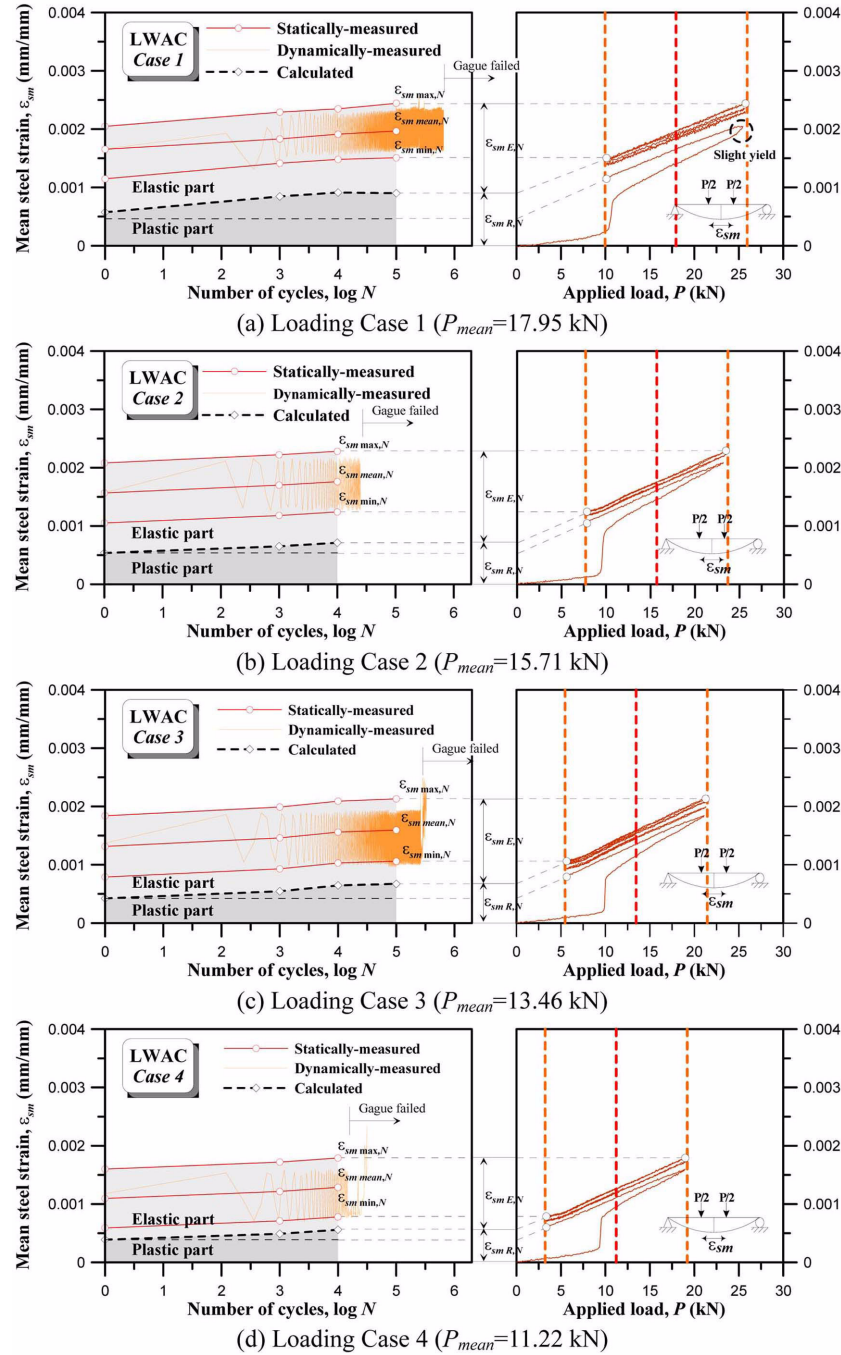
(d) Loading Case 4 (P_{mean}=11.22 kN)

Fig. 9 Fatigue test results for LWAC beams at various cyclic load levels

comparisons between LWAC and NWC beams clearly showed that the *applied load-mean steel strain* curves for the LWAC beams were more linear than those for the NWC beams. This indicated

(a) Loading Case 1 (P_{mean}=17.95 kN)

(b) Loading Case 2 (P_{mean}=15.71 kN)

(c) Loading Case 3 (P_{mean}=13.46 kN)
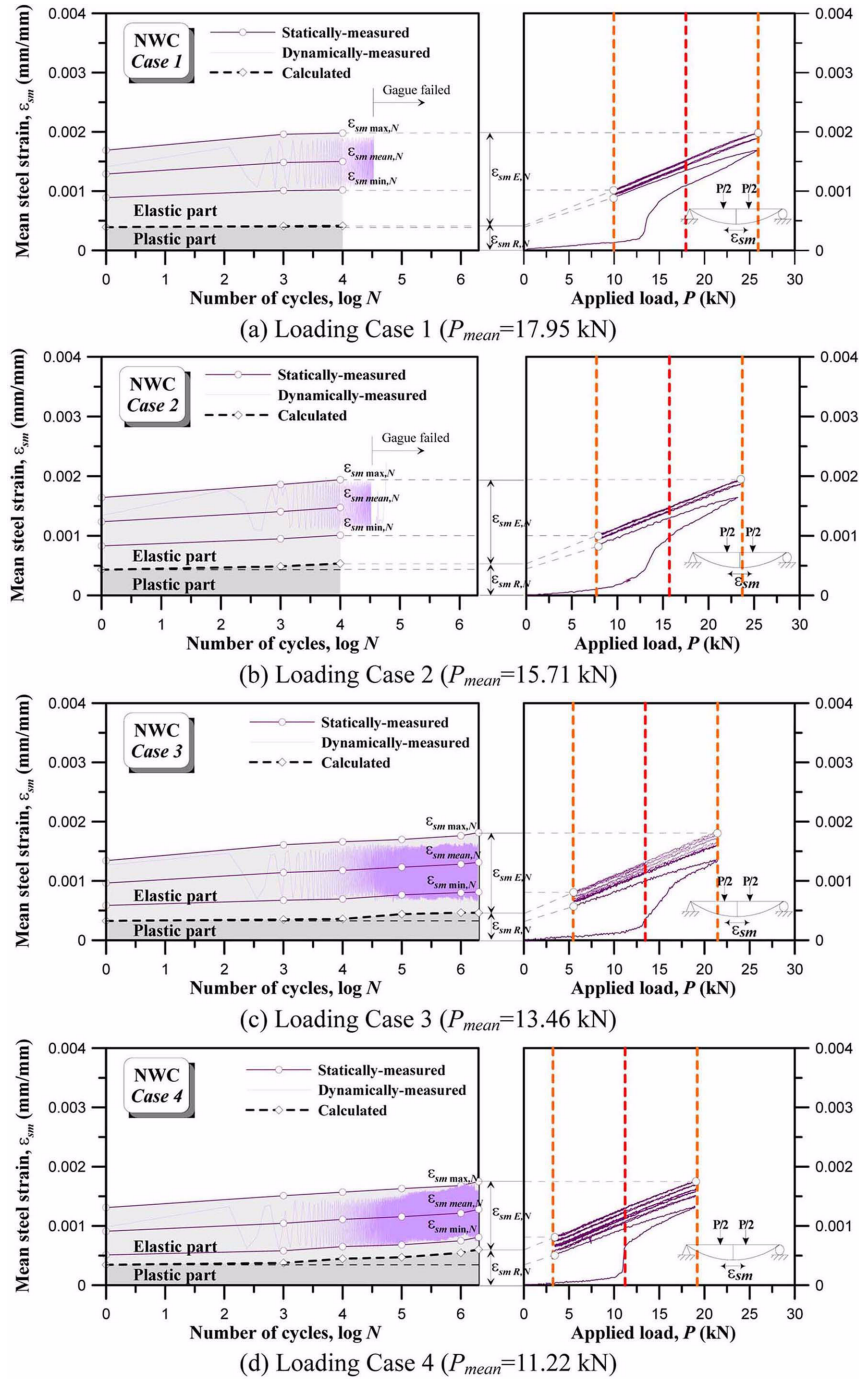
(d) Loading Case 4 (P_{mean}=11.22 kN)

Fig. 10 Fatigue test results for NWC beams at various cyclic load levels

that the LWAC beams depended more on the reinforcement to carry tensile forces and experienced less of a decrease in tension stiffening during cyclic actions.
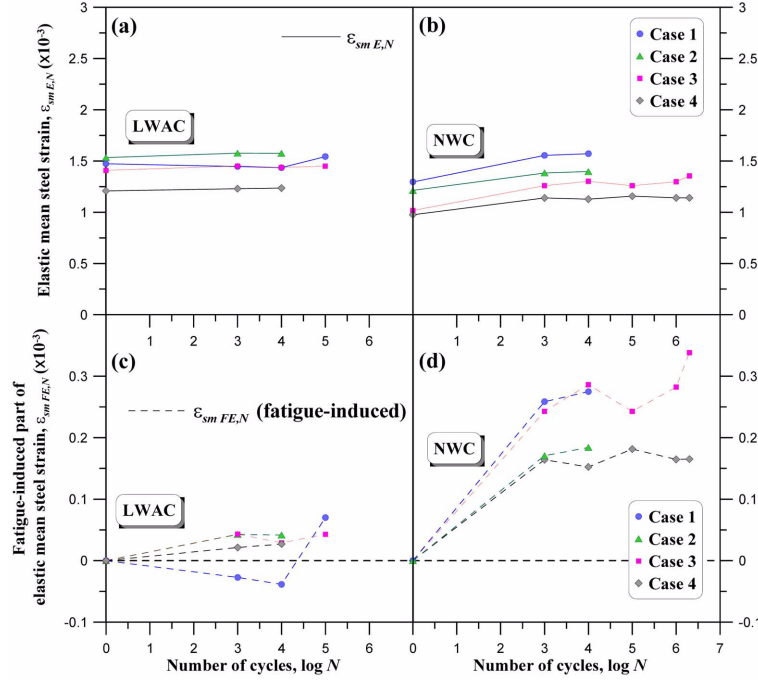
Fig. 11 Development of elastic mean steel strain with load cycles

Detailed descriptions of the mean steel strains, including both the elastic and residual parts, of RC beams are provided in the following sections.

4.2.2 Elastic mean steel strain ($\varepsilon_{smE,N}$)

Fig. 11 shows the development of elastic mean steel strain in the RC beams for a given available number of cycles, as calculated by the following equation

$$\varepsilon_{smE,N} = \frac{P_{\max}}{K_{smE,N}} \qquad (6)$$

where, $P_{\max}$ is the maximum cyclic load (Table 5); and $K_{smE,N}$ is the secant slope of the *applied load-mean steel strain* curve based on the two endpoints of the unloading stage at N cycles (Fig. 4). $K_{smE,N}$ is calculated by the following equation

$$K_{smE,N} = \frac{P_r}{\Delta\varepsilon_{sm,N}} \qquad (7)$$

where, P_r is the applied range of cyclic loads (Table 5); and $\Delta\varepsilon_{sm,N}$ is the measured range of mean steel strain at N cycles.

In Fig. 11, elastic mean steel strains at the last available cycles were between 1,236 and 1,575 μ for LWAC beams (Fig. 11(a)) and between 1,140 and 1,571 μ for NWC beams (Fig. 11(b)). Although higher elastic mean strains were observed in the LWAC beams due to a higher contribution of initial parts, the fatigue-induced parts were much smaller than those in the NWC beams (Figs. 11(c) and (d)). For all cyclic load levels, the development of elastic mean steel strain

in the LWAC beams remained nearly constant during fatigue testing. The increments of elastic mean steel strain with load cycles were mainly related to the decayed tension stiffening of concrete and the fatigue damage of the reinforcements, which was evaluated based on degradation of the elastic modulus. Although prior experimental results for cyclic strains of reinforcing steels are scarce, results for metals and thin wires can be used to determine that the elastic modulus of reinforcing steel (E_s) is cyclically stable within service load levels (Teng and Wang 2001). Therefore, based on results for the LWAC beams, the stability of the elastic mean steel strains during fatigue tests implied that there was less of a reduction in tension stiffening (i.e., a smaller local slip between steel and concrete resulting from bond degradation).

With the exception of the cyclic load level of Case 1, a slight yield occurred in the tensile steel of the LWAC beam when the applied load approached the maximum cyclic load (P_{max}) in the first cycle (Fig. 9(a)) because the maximum cyclic load of Case 1 was relatively close to the average yield load (P_y) for the LWAC beams. The elastic mean steel strain seemed to be suppressed due to the yield of tensile steel.

4.2.3 Residual mean steel strain ($\varepsilon_{smR,N}$)

Fig. 12 shows the development of residual mean steel strain in the RC beams over the available number of cycles. For a specific number of cycles, the residual mean steel strain was derived from Eq. 4 by subtracting the elastic mean steel strain from the total response. The residual mean steel strains at the last available cycle ranged from 558 to 901 μ for LWAC beams (Fig. 12(a)) and from 413 to 606 μ for NWC beams (Fig. 12(b)). The fatigue-induced increments of residual mean steel strain in the LWAC beams (Fig. 12(c)) were higher than those in the NWC beams (Fig. 12(d)) for
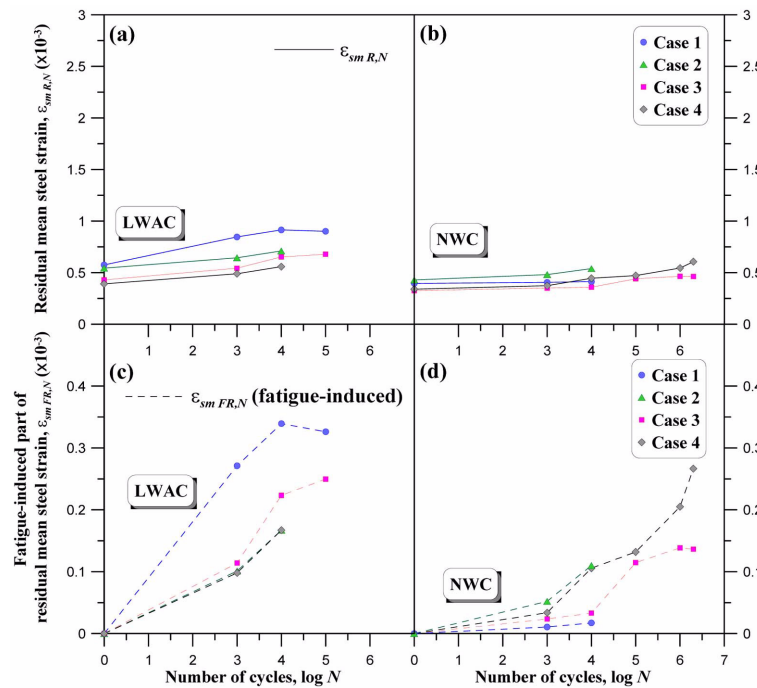

Fig. 12 Development of residual mean steel strain with load cycles

all cyclic load levels. Testing the RC beams at the cyclic load level of Case 1 resulted in the highest and lowest fatigue-induced strain increments in the LWAC and NWC beams, respectively.

The influence of tension stiffening on the development of residual mean steel strain in the LWAC beams was different from that in the NWC beams. For LWAC beams, the residual mean steel strain generally originated from the localized plasticity of reinforcement at the primarily flexural cracks due to better bonds between steel and concrete. At the location of a flexural crack, higher local steel stress (Fig. 3(b)) likely produced an earlier occurrence of localized plasticity. In LWAC beams, the tensile steel with a higher distributed mean steel stress and a reduced average yield strength (Fig. 7) tended to develop a higher residual mean steel strain with load cycles.

NWC beams had larger decreases in tension stiffening between adjacent flexural cracks with cyclic loads because of the higher fatigue-induced elastic mean steel strains (Fig. 11(d)). The residual mean steel strains developed in the NWC beams were mainly caused by the irreversible relative slip between steel and concrete. Compared to LWAC beams, a lower distributed mean steel stress and a smaller reduction in the average yield strength of tensile steel in the NWC beams (Fig. 7) led to a lower residual mean steel strain. Moreover, because the tensile steel behaved elastically at service load levels, the residual steel strains accumulated between flexural cracks (resulting from the residual local slip) were able to be released with the progressive interfacial debonding between steel and concrete. In particular, for the cyclic load level of Case 1 (Fig. 12(d)), the relatively larger magnitude of the cyclic load with a relatively greater decrease in tension stiffening prevented the residual mean steel strains from developing.
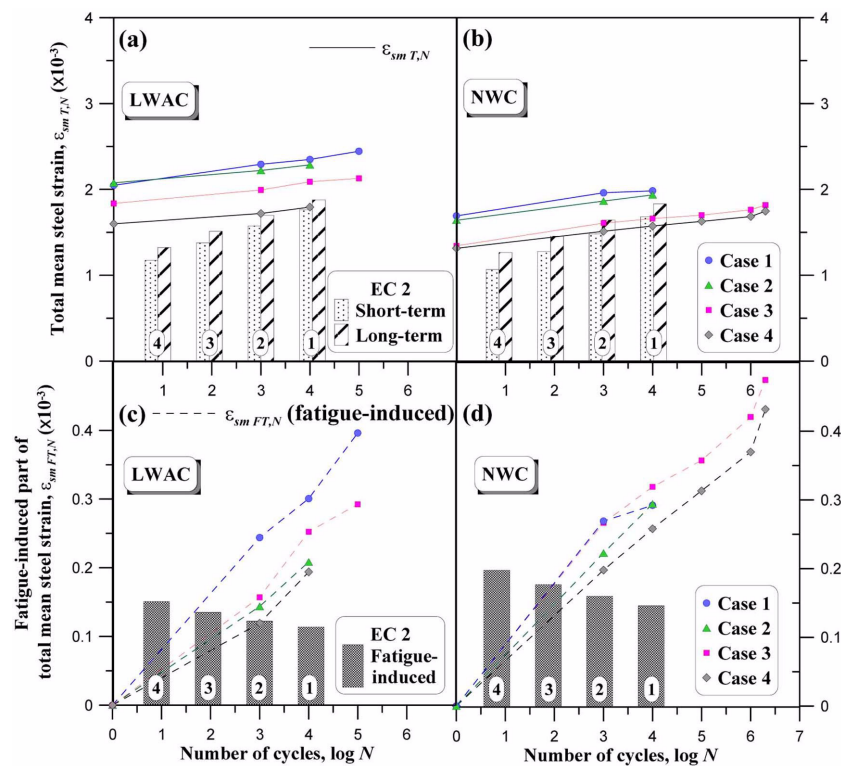

Fig. 13 Development of total mean steel strain with load cycles compared to EC 2

4.2.4 Total mean steel strain ($\varepsilon_{smT, N}$)

Comparisons of total mean steel strain developments and the calculated total responses based on the Eurocode 2 (EC 2) method are shown in Fig. 13. The measured total mean steel strain at the last available cycles ranged between 1,793 and 2,444 μ for the LWAC beams (Fig. 13(a)) and between 1,746 and 1,984 μ for the NWC beams (Fig. 13(b)). Except for the cyclic load level of Case 1, the LWAC beams had smaller fatigue-induced increments of total mean steel strain than the NWC beams under the same cyclic load levels (Figs. 13(c) and (d)). As discussed previously, higher fatigue-induced increments in the LWAC beam for Case 1 were due to higher localized plasticity at the location of primary flexural cracks (Fig. 12(c)). A slight yield of the tensile steel occurred in the first cycle (Fig. 9(a)). This cannot be explained solely based on the total response due to the complex nature of concrete cracking. With the method proposed in Section 3.2, a better understanding of the high-cycle fatigue problem for RC beams was provided. Additionally, whether or not the effects of long-term or repeated loads were taken into account, the calculated values of total response, based on the EC 2 method, were lower than the experiment results for all cyclic load levels (Fig. 13). Particularly, there was a higher deviation for LWAC beams. In contrast to the experimental results, the predictions from the EC 2 method were considered non-conservative.

5. Conclusions

An experimental study of the tension stiffening behavior of LWAC and NWC beams with equal compressive strengths subjected to high-cycle fatigue loading was conducted. The following conclusions were drawn:

1. Compared to NWC beams, LWAC beams behaved more linearly in the *applied load-mean steel strain* curves. This indicated that LWAC beams experienced less of a decrease in tension stiffening and depended more on the reinforcement to carry the tension force.

2. Improved tension stiffening in LWAC beams under cyclic loading was confirmed by the stability of the elastic mean steel strains during fatigue testing.

3. The LWAC beams tended to develop higher residual mean steel strains at the primary flexural cracks (localized plasticity), whereas the residual mean steel strains developed in the NWC beams could be released by progressive debonding between steel and concrete.

4. With the exception of the cyclic load level of Case 1, in which a slight yield of tensile steel occurred in the first cycle, the LWAC beams had smaller fatigue-induced increments of total mean steel strain than the NWC beams under the same cyclic load levels.

5. In contrast to the experiment results, the total mean steel strains predicted from the EC 2 method were on the non-conservative side, whether or not the effects of long-term or repeated loads were taken into account. A higher deviation was observed for LWAC beams.

Acknowledgments

References

ACI Committee 213 (2003), *Guide for Structural Lightweight Aggregate Concrete (ACI 213R-03)*, American Concrete Institute, Michigan.

ACI Committee 215 (1992), *Considerations for Design of Concrete Structures Subjected to Fatigue Loading (ACI 215R-92)*, American Concrete Institute, Detroit.

ACI Committee 318 (2005), *Building Code Requirements for Structural Concrete (ACI 318-05) and Commentary (318R-05)*, American Concrete Institute, Michigan.

ACI Committee 408 (1992), *State-of-the-Art-Report: Bond Under Cyclic Loading (ACI 408.2R-92)*, American Concrete Institute, Michigan.

Balaguru, P. and Shah, S.P. (1982), "A method of predicting crack widths and deflections for fatigue loading", *Fatigue of Concrete Structures (ACI SP-75)*, American Concrete Institute, Detroit.

CEB (1993), *CEB-FIP Model Code 1990 (Concrete Structures)*, Comité Euro-International du Béton, Lausanne, Switzerland.

CEN (2004), *Eurocode 2 : Design of Concrete Structures, Part 1.1: General Rules and Rules for Buildings (EN 1992-1-1)*, European Committee for Standardization, Brussels, Belgium.

Chen, H.J., Huang, C.H. and Kao, Z.Y. (2004), "Experimental investigation on bond between concrete and bar", *Struct. Eng. Mech.*, **17**(2), 141-152.

Cornelissen, H.A.W., Hordijk, D.A. and Reinhardt, H.W. (1986), "Experimental determination of crack softening characteristics of normalweight and lightweight concrete", *Heron*, **31**(2), 45-56.

Dede, T. and Ayvaz, Y. (2009), "Nonlinear analysis of reinforced concrete beam with/without tension stiffening effect", *Mater. Des.*, **30**(9), 3846-3851.

Fantilli, A.P. and Vallini, P. (2004), "Strains in steel bars of reinforced concrete elements subjected to repeated loads", *J. Strain Anal. Eng. Des.*, **39**(5), 447-457.

Fib (2000), *Bond of Reinforcement in Concrete (Bulletin 10)*, State-of-art report, Federation International du Beton, Lausanne, Switzerland.

Ganesh Babu, K. (1979), "Mean steel strain in reinforced concrete flexural members", *Mater. Struct.*, **12**(3), 207-214.

Hossain, K.M.A. (2008), "Bond characteristics of plain and deformed bars in lightweight pumice concrete", *Constr. Build. Mater.*, **22**(7), 1491-1499.

Ke, Y., Beaucour, A.L., Ortola, S., Dumontet, H. and Cabrillac, R. (2009), "Influence of volume fraction and characteristics of lightweight aggregates on the mechanical properties of concrete", *Constr. Build. Mater.*, **23**(8), 2821-2828.

Koch, R. and Balázs, G.L. (1992), "Influence of cyclic loading on bond strength and related slip", *Proceedings of the Bond in Concrete Conference*, Riga.

Lachemi, M., Bae, S., Hossain, K.M.A. and Sahmaran, M. (2009), "Steel-concrete bond strength of lightweight self-consolidating concrete", *Mater. Struct.*, **42**(7), 1015-1023.

Lenschow, R. (1982), "Fatigue of concrete structures", *Fatigue of Steel and Concrete Structures*, Proceedings IABSE Reports (Vol. 37), International Association for Bridge and Structural Engineering, Lausanne, Switzerland.

Lovegrove, J.M. and EI Din, S. (1982), "Deflection and cracking of reinforced concrete under repeated loading and fatigue", *Fatigue of Concrete Structures (ACI SP-75)*, American Concrete Institute, Detroit.

Maekawa, K., Pimanmas, A. and Okamura, H. (2003), *Nonlinear Mechanics of Reinforced Concrete*, Taylor & Francis Group.

Mor, A. (1992), "Steel-concrete bond in high-strength lightweight concrete", *ACI Mater. J.*, **89**(1), 76-82.

Mor, A., Gerwick, B.C. and Hester, W.T. (1992), "Fatigue of high-strength reinforced concrete", *ACI Mater. J.*, **89**(2), 197-207.

Mouli, M. and Khelafi, H. (2008), "Performance characteristics of lightweight aggregate concrete containing natural pozzolan", *Build. Environ.*, **43**(1), 31-36.

Oh, B.H., Cho, J.Y. and Park, D.G. (2003), "Static and fatigue behavior of reinforced concrete beams strengthened with steel plates for flexure", *J. Struct. Eng.-ASCE*, **129**(4), 527-535.

Stramandinoli, R.S.B. and Rovere, H.L.L. (2008), "An efficient tension-stiffening model for nonlinear analysis of

reinforced concrete members", *Eng. Struct.*, **30**(7), 2069-2080.

Teng, S. and Wang, F. (2001), "Finite element analysis of reinforced concrete deep beams under fatigue loading", *ACI Struct. J.*, **98**(3), 315-323.

Zanuy, C., Albajar, L. and de la Fuente, P. (2009), "On the cracking behaviour of the reinforced concrete tension chord under repeated loading", *Mater. Struct.*, **43**(5), 611-632.

Zanuy, C., de la Fuente, P. and Albajar, L. (2010), "Estimation of parameters defining negative tension stiffening", *Eng. Struct.*, **32**(10), 3355-3362.

Notations

P	= applied load
P_{cr}, P_y	= cracking and yield load
P_{max}, P_{mean}, P_{min}	= maximum, mean and minimum cyclic load
P_r	= range of cyclic load
ε_{sm}	= mean steel strain
σ_{sm}	= mean steel stress
ε_{s1}, ε_{s2}	= steel strains in States 1 and 2
ζ	= dimensionless coefficient representing the extent of cracking
$\sigma_{s,cr}$, σ_s	= stresses in the tensile steel, calculated on the basis of a fully cracked section under the cracking load P_{cr} and the load P
β_1, β_2	= parameters to account for bond characteristics and the nature of the loads
a	= shear span length
d	= effective depth from the extreme compressive fiber to the centroid of the tensile steel
i	= subscript to represent the member state ($i=1$ for State 1 and $i=2$ for State 2)
y_i	= distance from the extreme compressive fiber to the neutral axis in State i
I_i	= moment of inertia of the transformed section in State i
E_s	= elastic modulus of the reinforcement
n	= modular ratio of reinforcement to concrete
λ	= symbol to represent the total ($\lambda \to T$), elastic ($\lambda \to E$) and residual ($\lambda \to R$) mean steel strains
N	= number of load cycles
$\varepsilon_{smE,N}$, $\varepsilon_{smR,N}$, $\varepsilon_{smT,N}$	= elastic, residual and total mean steel strains at N cycles
ε_{smIE}, ε_{smIR}, ε_{smIT}	= initial elastic, residual and total mean steel strains (first cycle)
$\varepsilon_{smFE,N}$, $\varepsilon_{smFR,N}$, $\varepsilon_{smFT,N}$	= fatigue-induced elastic, residual and total mean steel strains at N cycles
$\Delta\varepsilon_{sm,N}$	= range of mean steel strain at N cycles
$K_{sm,N}$	= secant slope of the *applied load-mean steel strain* curve based on the two endpoints of the unloading stage at N cycles